



ELSEVIER

Journal of Alloys and Compounds 298 (2000) 119–124

Journal of
ALLOYS
AND COMPOUNDS

www.elsevier.com/locate/jallcom

Structure and cation distribution of new ternary vanadates $\text{FeMg}_2\text{V}_3\text{O}_{11}$ and $\text{FeZn}_2\text{V}_3\text{O}_{11}$

Xiandong Wang, Douglas A. Vander Griend, Charlotte L. Stern, Kenneth R. Poeppelmeier*

Department of Chemistry, Northwestern University, Evanston IL, 60208-3113, USA

Received 2 August 1999; received in revised form 21 October 1999; accepted 21 October 1999

Abstract

$\text{FeMg}_2\text{V}_3\text{O}_{11}$ crystals grown from a $\text{MgO}/\text{Fe}_2\text{O}_3/\text{V}_2\text{O}_5$ melt crystallize in the triclinic space group $P-1$ with parameters: $a=6.434(1)$ Å, $b=6.806(1)$ Å, $c=10.085(1)$ Å, $\alpha=97.44(1)^\circ$, $\beta=103.44(1)^\circ$, $\gamma=101.56(1)^\circ$ and $Z=2$. $\text{FeZn}_2\text{V}_3\text{O}_{11}$ crystals grown from a $\text{ZnO}/\text{Fe}_2\text{O}_3/\text{V}_2\text{O}_5$ melt also crystallize in $P-1$ with similar parameters: $a=6.455(1)$ Å, $b=6.834(1)$ Å, $c=9.988(1)$ Å, $\alpha=97.65(1)^\circ$, $\beta=102.61(1)^\circ$, $\gamma=101.26(1)^\circ$ and $Z=2$. Both are isostructural with $\text{GaZn}_2\text{V}_3\text{O}_{11}$, and susceptibility measurements reveal that all iron is high spin d^5 . In $\text{FeMg}_2\text{V}_3\text{O}_{11}$, Fe^{3+} is distributed non-statistically with Mg^{2+} on octahedral and bipyramidal sites. In $\text{FeZn}_2\text{V}_3\text{O}_{11}$, Fe^{3+} is found only on the octahedral sites and Zn^{2+} exclusively occupies the bipyramidal sites. © 2000 Published by Elsevier Science S.A. All rights reserved.

Keywords: Vanadate; Ferrate; Single crystal; Structure; Cation disorder

1. Introduction

Multicomponent molybdates and vanadates are known to catalyze a variety of selective hydrocarbon oxidations. Previous work on the $\text{MO}-\text{V}_2\text{O}_5-\text{MoO}_3$ ($\text{M}=\text{Mg}, \text{Zn}, \text{Mn}$) systems [1–4] revealed a series of vanadomolybdates: $\text{M}_{2.5}\text{VMoO}_8$ ($\text{M}=\text{Mg}^{2+}, \text{Zn}^{2+}, \text{Mn}^{2+}$) which demonstrate remarkable solid-state chemistry. $\text{Mg}_{2.5}\text{VMoO}_8$ in particular shows good selectivity for the oxidative dehydrogenation of butane [5]. While this heterogeneous gas–solid reaction occurs on the surface, detailed understanding of the structure and defects of the bulk of this catalyst unveiled aspects of the complex chemistry involved. The structure of all these vanadomolybdates features one dimensional columns built of face-sharing octahedra and isolated $(\text{V}/\text{Mo})\text{O}_4$ tetrahedra, similar to such molybdates as $\text{NaCo}_{2.31}(\text{MoO}_4)_3$ [6], $\text{Cu}_{3.85}(\text{MoO}_4)_3$ [7], and $(\text{Cu},\text{Zn})_{3.75}(\text{MoO}_4)_3$ [8]. The only vanadate without molybdenum to adopt these features is naturally occurring $\alpha\text{-Cu}_3\text{Fe}_4(\text{VO}_4)_6$ (lyonsite) [9] of which $\text{Mg}_{2.5}\text{VMoO}_8$ is a homeotype [3]. The synthesized structure however, $\beta\text{-Cu}_3\text{Fe}_4(\text{VO}_4)_6$, while it has isolated VO_4 tetrahedra, does not have chains of face-sharing octahedra [10]. Our understanding of the aforementioned vanadomolybdate catalysts advocates searching for new vanadates, especially those with chains of face-sharing octahedra and isolated VO_4 tetrahedra. It should be possible to find new ternary vanadates with comparable structures by replacing the Cu in $\alpha\text{-Cu}_3\text{Fe}_4(\text{VO}_4)_6$ with other divalent metals. The $\text{MO}-\text{Fe}_2\text{O}_3-\text{V}_2\text{O}_5$ ($\text{M}=\text{Mg}, \text{Zn}, \text{Co}$ and Mn) systems were consequently selected for investigation since these divalent metals are the ones which occur in the vanadomolybdates. To facilitate the discovery and characterization of new metal oxides, single crystals were grown from ternary fluxes. This technique not only leads to precise structural solutions, but also elucidates reactions which lead to the phases in the ternary system. In the first two systems, the ternary compounds $\text{FeMg}_2\text{V}_3\text{O}_{11}$ and $\text{FeZn}_2\text{V}_3\text{O}_{11}$ were discovered to adopt yet another structure, the $\text{GaZn}_2\text{V}_3\text{O}_{11}$ -type structure, with VO_4 tetrahedra and VO_5 bipyramids. This paper reports structural details along with magnetic and spectroscopic measurements for these two compounds. Exploration of the last two systems yielded the new compounds $\text{Co}_4\text{Fe}_{3.33}(\text{VO}_4)_6$ and $\text{Mn}_3\text{Fe}_6(\text{VO}_4)_6$ which adopt the $\alpha\text{-Cu}_3\text{Fe}_4(\text{VO}_4)_6$ and $\beta\text{-Cu}_3\text{Fe}_4(\text{VO}_4)_6$ struc-

*Corresponding author. Fax: +1-847-491-7713.

E-mail address: krp@nwu.edu (K.R. Poeppelmeier)

tures, respectively. These will be reported in a subsequent paper [11].

2. Experimental

Polycrystalline $\text{FeMg}_2\text{V}_3\text{O}_{11}$ was prepared from a stoichiometric mixture of Fe_2O_3 (Aldrich, 99+%), MgO (Aldrich, 98%), and V_2O_5 (Aldrich, 99.6+%). The samples were ground in an agate mortar, calcined at 650°C for 24 h in an alumina boat, and pressed into pellets. They were reacted at $750\text{--}780^\circ\text{C}$ for 60 h and then at 900°C for 44 h followed by quenching in air. Polycrystalline $\text{FeZn}_2\text{V}_3\text{O}_{11}$ was similarly prepared from Fe_2O_3 , ZnO (Aldrich, 99.99%) and V_2O_5 . The samples were reacted at 700°C for 10 h and then at 750°C for 48 h followed by quenching in air. No impurities are observed in X-ray powder patterns, and the melting points of the green $\text{FeMg}_2\text{V}_3\text{O}_{11}$ and yellow $\text{FeZn}_2\text{V}_3\text{O}_{11}$ powders were determined by differential thermal analysis (DTA) in air to be $1015\pm 2^\circ\text{C}$ and $851\pm 2^\circ\text{C}$, respectively.

$\text{FeMg}_2\text{V}_3\text{O}_{11}$ crystals were grown from a mixture of 1.756 g Fe_2O_3 , 0.665 g MgO , and 3 g V_2O_5 , which corresponds to the nominal composition $\text{Mg}_3\text{Fe}_4(\text{VO}_4)_6$. The mixture was ground in an agate mortar, packed in a Pt crucible, and calcined at 700°C for 18 h. It was then heated to 1050°C at 180°C h^{-1} , held at 1050°C for 2 h, cooled slowly to 850°C at 6°C h^{-1} , and finally cooled to room temperature at 60°C h^{-1} . The observed weight loss of the total flux was 1.7%. Dark crystals 0.2–1.0 mm in size were obtained by breaking apart the melt. The atomic ratios (Fe:Mg:V=1.0:2.0:2.7) determined by energy dispersive analysis of X-rays (EDAX) confirm the stoichiometry of this new compound.

$\text{FeZn}_2\text{V}_3\text{O}_{11}$ crystals were obtained using a mixture containing 2.207 g Fe_2O_3 , 2.529 g ZnO , and 4.396 g V_2O_5 which corresponds to the nominal composition $\text{Zn}_{3.86}\text{Fe}_{3.43}(\text{VO}_4)_6$. The mixture was packed in a Pt crucible and reacted at 920°C for 1 h. The melt was slowly cooled to 710°C at 6°C h^{-1} and subsequently cooled to room temperature at 60°C h^{-1} . The total weight loss was about 1%. Brown–yellow plates and bright yellow plates were obtained and identified by EDAX to be $\text{FeZn}_2\text{V}_3\text{O}_{11}$ (Fe:Zn:V=1.0:1.8:2.9) and V_2O_5 , respectively.

Infrared spectra of polycrystalline $\text{FeMg}_2\text{V}_3\text{O}_{11}$ and $\text{FeZn}_2\text{V}_3\text{O}_{11}$ with KBr were obtained over the range of $4400\text{--}400\text{ cm}^{-1}$ and recorded on a Bio-Rad FT-IR spectrophotometer at 2.0 cm^{-1} increments for 30 scans. Magnetic susceptibility data were collected on a SQUID susceptometer (Quantum Design, MPMS) at 1kG between 5 and 300 K. About 27 mg $\text{FeMg}_2\text{V}_3\text{O}_{11}$ and 31 mg $\text{FeZn}_2\text{V}_3\text{O}_{11}$ powders were sealed in gelatin capsules and zero-field-cooled to 5 K. Corrections for core diamagnetism were applied [12].

The same crystals used for EDAX were mounted on glass fibers for study by single crystal X-ray diffraction.

Table 1
Crystallographic data^a

Chemical formula	$\text{FeMg}_2\text{V}_3\text{O}_{11}$	$\text{FeZn}_2\text{V}_3\text{O}_{11}$
Formula weight	433.27	515.42
Space group	<i>P</i> -1	<i>P</i> -1
<i>a</i> , Å	6.434(1)	6.455(1)
<i>b</i> , Å	6.806(1)	6.834(1)
<i>c</i> , Å	10.085(1)	9.988(1)
α , deg	97.44(1)	97.65(1)
β , deg	103.44(1)	102.61(1)
γ , deg	101.56(1)	101.26(1)
<i>V</i> , Å ³	413.6(1)	414.5(1)
<i>Z</i>	2	2
ρ_{calc} , g cm ⁻³	3.479	4.129
<i>R</i> ^b	0.030	0.040
<i>R</i> _w ^c	0.041	0.062

^a Further details of the crystal structure determination can be ordered from Fachinformationszentrum Karlsruhe, 76344 Eggenstein–Leopoldshafen, under the depository numbers CSD-410983 and CSD-410984.

$$^b R = \frac{\sum ||F_o| - |F_c||}{\sum |F_o|}$$

$$^c R_w = \left[\frac{\sum w(|F_o| - |F_c|)^2}{\sum w|F_o|^2} \right]^{1/2}, w = 1/\sigma^2(F_o)$$

All measurements were made on an Enraf–Nonius CAD4 diffractometer with graphite monochromated Mo- K_α radiation. The unit cell parameters were determined by a least-squares fit using the setting angles of 25 centered reflections in the ranges of $21.9 \leq 2\theta \leq 25.7$ for $\text{FeMg}_2\text{V}_3\text{O}_{11}$ and $20.1 \leq 2\theta \leq 23.1$ for $\text{FeZn}_2\text{V}_3\text{O}_{11}$. Both an analytical absorption correction [13] and a secondary extinction correction were made. Lorentz and polarization effects were taken into account. Both structures were solved by direct methods with SHELXS86 [14] and DIRDIF94 [15] and refined on $|F|$ with TEXSAN [16] by least-squares. All atoms were refined anisotropically except for the disordered metal atoms. A summary of crystallographic data is provided in Table 1, and atomic parameters for $\text{FeMg}_2\text{V}_3\text{O}_{11}$ and $\text{FeZn}_2\text{V}_3\text{O}_{11}$ are given in Tables 2 and 3, respectively.

3. Results and discussion

$\text{FeZn}_2\text{V}_3\text{O}_{11}$ and $\text{FeMg}_2\text{V}_3\text{O}_{11}$ are isostructural with $\text{GaMg}_x\text{Zn}_{2-x}\text{V}_3\text{O}_{11}$ ($x=0, 1.7$) [17,18]. The structure is built up from $\text{M}(1)\text{O}_6$ and $\text{M}(2)\text{O}_6$ octahedra, $\text{M}(3)\text{O}_5$ and $\text{V}(2)\text{O}_5$ trigonal bipyramids, and two types of VO_4 tetrahedra (Fig. 1). $\text{V}(1)\text{O}_4$ is an isolated tetrahedron, while the remaining vanadium–oxygen species consists of $\text{V}_4\text{O}_{14}^{8-}$ clusters. Each cluster contains two edge-shared $\text{V}(2)\text{O}_5$ bipyramids which each share a corner oxygen with a $\text{V}(3)\text{O}_4$ tetrahedron (Fig. 2b). It is worthwhile to note that V^{5+}O_5 trigonal bipyramidal coordination is not common [19,20]. The $\text{M}(1)\text{O}_6$, $\text{M}(2)\text{O}_6$ and $\text{M}(3)\text{O}_5$ linkages are shown in Fig. 2a. Each $\text{M}(3)\text{O}_5$ bipyramid shares an edge with one $\text{M}(2)\text{O}_6$ octahedron and a corner with one $\text{M}(1)_2\text{O}_{10}$ octahedral dimer. Similar iron–oxygen polyhedral units are found in FeVO_4 [21], but in that case the

Table 2
Atomic parameters for $\text{FeMg}_2\text{V}_3\text{O}_{11}$

Atom	Position	x	y	Z	$U_{\text{eq}}/U_{\text{iso}}^{\text{a}}$
M1 ^b	2i	0.3054(1)	0.8263(1)	0.49511(7)	0.0038(2) ^c
M2 ^c	2i	0.2392(1)	0.4941(1)	0.22707(7)	0.0031(2) ^c
M3 ^d	2i	-0.1739(2)	0.1243(2)	0.1648(1)	0.0030(2) ^c
V(1)	2i	-0.32948(9)	-0.01092(9)	-0.20691(6)	0.0038(1)
V(2)	2i	-0.30669(9)	0.57194(9)	0.12270(6)	0.0035(1)
V(3)	2i	0.26392(9)	0.32938(9)	0.53218(6)	0.0034(1)
O(1)	2i	-0.6111(4)	-0.1246(4)	-0.2843(3)	0.0063(6)
O(2)	2i	-0.2576(4)	0.2042(4)	-0.2768(3)	0.0060(6)
O(3)	2i	-0.3058(4)	0.0700(4)	-0.0413(3)	0.0099(6)
O(4)	2i	-0.1948(4)	-0.1854(4)	0.1530(3)	0.0075(6)
O(5)	2i	-0.1055(4)	0.4394(4)	0.1658(3)	0.0063(6)
O(6)	2i	0.1589(4)	0.1855(4)	0.2143(3)	0.0072(6)
O(7)	2i	0.3708(4)	0.4913(4)	0.0671(3)	0.0079(6)
O(8)	2i	0.3716(4)	0.1254(4)	0.4831(3)	0.0053(6)
O(9)	2i	0.2819(4)	0.5232(4)	0.4362(3)	0.0064(6)
O(10)	2i	0.3958(4)	0.4388(4)	0.7037(3)	0.0075(6)
O(11)	2i	-0.0040(4)	0.7751(4)	0.4847(3)	0.0114(6)

^a U_{eq} is defined as one-third of the trace of the orthogonalized U_{ij} tensor.

^b M1=0.45Fe+0.55Mg.

^c M2=0.45Fe+0.55Mg.

^d M3=0.10Fe+0.90Mg.

^e U_{iso} .

FeO_5 bipyramid shares an edge with both the FeO_6 octahedra and the Fe_2O_{10} octahedral dimer.

The distribution of the Mg, Zn, and Fe atoms was established by examining the results of least-squares refinements and bond valence calculations. To avoid negative temperature factors in $\text{FeMg}_2\text{V}_3\text{O}_{11}$ the iron atoms had to be disordered with magnesium atoms on all three possible sites [M(1), M(2), and M(3)]. Site-indepen-

dent population refinements gave rise to the distributions M(1)=0.461(5)Fe+0.539(5)Mg, M(2)=0.467(5)Fe+0.533(5)Mg, and M(3)=0.128(5)Fe+0.872(5)Mg. Since the refinement program cannot simultaneously constrain

Table 3
Atomic parameters for $\text{FeZn}_2\text{V}_3\text{O}_{11}$

Atom	Position	x	y	z	$U_{\text{eq}}/U_{\text{iso}}^{\text{a}}$
M1 ^b	2i	0.3068(2)	0.8255(1)	0.4983(1)	0.0030(4) ^c
M2 ^c	2i	0.2290(1)	0.4949(1)	0.2232(1)	0.0035(3) ^c
M3 ^d	2i	-0.1722(2)	0.1265(1)	0.1676(1)	0.0039(2)
V(1)	2i	-0.3270(2)	-0.0120(2)	-0.2065(2)	0.0020(3)
V(2)	2i	-0.3036(2)	0.5733(2)	0.1194(2)	0.0024(3)
V(3)	2i	0.2561(2)	0.3267(2)	0.5275(2)	0.0017(3)
O(1)	2i	-0.608(1)	-0.125(1)	-0.282(1)	0.005(1)
O(2)	2i	-0.257(1)	0.202(1)	-0.279(1)	0.005(1)
O(3)	2i	-0.303(1)	0.068(1)	-0.040(1)	0.008(1)
O(4)	2i	-0.190(1)	-0.187(1)	0.148(1)	0.008(1)
O(5)	2i	-0.104(1)	0.441(1)	0.157(1)	0.006(1)
O(6)	2i	0.158(1)	0.185(1)	0.218(1)	0.006(1)
O(7)	2i	0.378(1)	0.493(1)	0.072(1)	0.008(2)
O(8)	2i	0.372(1)	0.124(1)	0.483(1)	0.003(1)
O(9)	2i	0.284(1)	0.525(1)	0.434(1)	0.006(1)
O(10)	2i	0.371(1)	0.430(1)	0.698(1)	0.013(2)
O(11)	2i	0.005(1)	0.778(1)	0.496(1)	0.014(2)

^a U_{eq} is defined as one-third of the trace of the orthogonalized U_{ij} tensor.

^b M1=0.639(4)Fe+0.361(4) Zn.

^c M2=0.361(4)Fe+0.639(4) Zn.

^d M3=Zn.

^e U_{iso} .

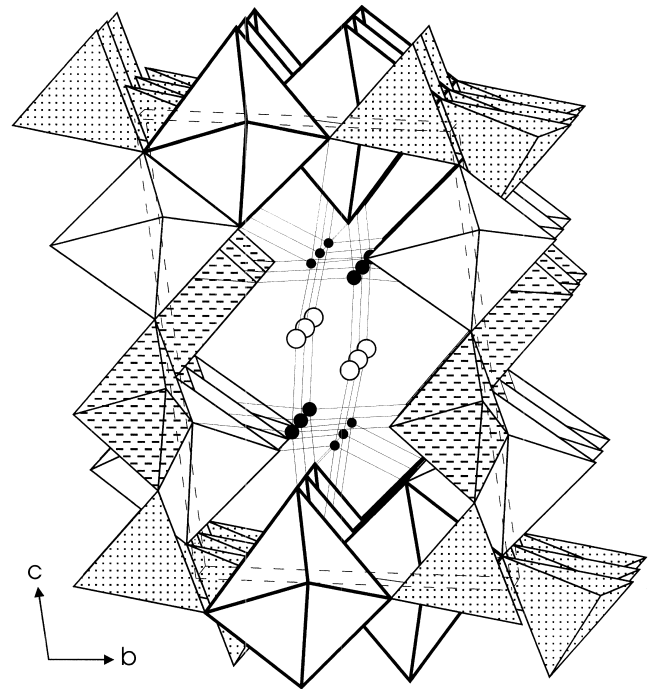


Fig. 1. Structure of $\text{FeM}_2\text{V}_3\text{O}_{11}$ (M=Mg and Zn). Small solid circle, V(1); medium solid circle, M3; large circle, O(3); octahedra in thick solid line, M1O_6 ; octahedra in thin solid line, M2O_6 ; bipyramids shaded with dashed line, V(2)O_5 ; tetrahedra shaded with dotted line, V(3)O_4 ; unit cell, dashed line frame. Configurations of M1, M2 and M3 are given in Tables 2 and 3.

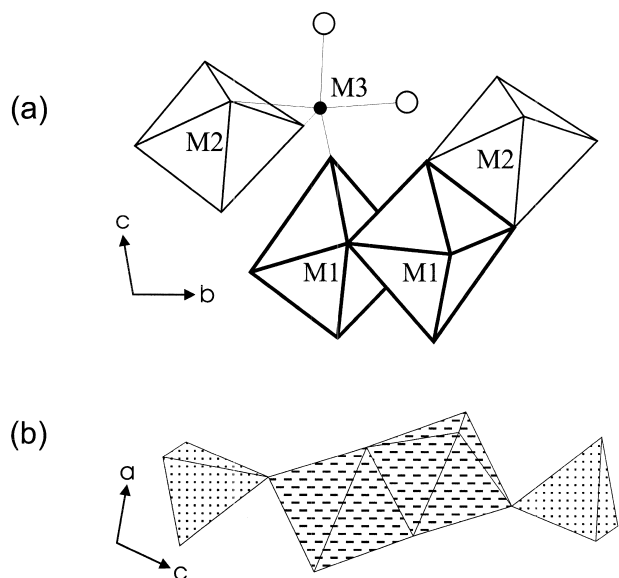


Fig. 2. (a) The linkage among M1O₆, M2O₆ and M3O₅ polyhedra. (b) V₄O₁₄⁸⁻ cluster formed by two V(2)O₅ trigonal bipyramids and two V(3)O₄ tetrahedra.

the total atomic ratio of Fe to Mg, the populations of the disordered atoms in the final refinements were fixed at the values given in Table 2 to balance the charge. The zinc analogue refinement required disordered iron atoms on only two sites, M(1)=0.639(4)Fe+0.361(4)Zn and M(2)=0.361(4)Fe+0.639(4)Zn, so the atomic ratio of Zn to Fe was simultaneously constrained to two. Table 3 gives the refined populations for all three sites.

Table 4 gives and compares notable bond lengths for FeMg₂V₃O₁₁ and FeZn₂V₃O₁₁. Among the differences, M(2)–O(10) ($\delta=+0.238$ Å) and M(2)–O(5) ($\delta=-0.049$ Å) have the largest absolute values, indicative of a significant difference in the degree of M(2)O₆ distortion between these two phases. This octahedral distortion can be estimated quantitatively using the equation: $\Delta = \frac{1}{6} \sum [(R_i - \bar{R})/\bar{R}]^2$, where R_i and \bar{R} are the individual and average bond lengths, respectively [22]. The calculated distortion of the M(2)O₆ octahedra in FeZn₂V₃O₁₁ ($\Delta \times 10^3 = 6.11$) is significantly larger than that in FeMg₂V₃O₁₁ ($\Delta \times 10^3 = 1.36$). This effect is ascribed to the zinc occupation of the M(2) sites (Table 3): the more zinc, the larger octahedral distortion. The M(2)O₆ octahedra are also more distorted than the M(1)O₆ ones in FeZn₂V₃O₁₁ ($\Delta \times 10^3 = 1.23$) as expected. The tendency of ZnO₆ octahedra to distort is well established [23–27].

Comparison of the unit cell parameters (Table 1) shows that the a and b axes increase while the c axis decreases with the increase of the divalent ion sizes ($r(\text{Mg}^{2+}) < r(\text{Zn}^{2+})$). The distortion of the polyhedra with the substitution of zinc for magnesium is believed responsible for the change in cell parameters. A similar relationship is observed between GaMg_{1.7}Zn_{0.3}V₃O₁₁ and GaZn₂V₃O₁₁ [17,18]. In both cases, the a axes of the zinc-rich analogue

Table 4

Selected bond lengths (Å) for FeM₂V₃O₁₁ (M=Mg, Zn)

Bond	M=Mg	M=Zn	$\delta(\text{Zn-Mg})$
M1–O(1)	2.128(3)	2.102(6)	–0.026
M1–O(2)	2.127(2)	2.123(6)	–0.004
M1–O(8)	1.993(2)	1.995(6)	0.002
M1–O(8)	2.020(2)	2.035(5)	0.015
M1–O(9)	2.037(2)	2.035(6)	–0.002
M1–O(11)	1.926(3)	1.907(6)	–0.019
M2–O(2)	2.022(3)	2.032(6)	0.010
M2–O(5)	2.100(3)	2.051(6)	–0.049
M2–O(6)	2.039(3)	2.071(6)	0.032
M2–O(7)	1.988(3)	1.957(6)	–0.031
M2–O(9)	2.040(3)	2.035(6)	–0.005
M2–O(10)	2.222(3)	2.460(7)	0.238
M3–O(1)	2.034(2)	2.009(6)	–0.025
M3–O(3)	2.009(3)	2.015(7)	0.006
M3–O(4)	2.071(3)	2.103(6)	0.032
M3–O(5)	2.100(3)	2.131(5)	0.031
M3–O(6)	2.025(3)	2.027(6)	0.002
V(1)–O(1)	1.765(3)	1.777(6)	0.012
V(1)–O(2)	1.733(3)	1.740(6)	0.007
V(1)–O(3)	1.651(3)	1.643(7)	–0.008
V(1)–O(6)	1.777(3)	1.765(6)	–0.012
V(1)–O(8)	2.728(3)	2.700(6)	–0.028
V(2)–O(4)	1.622(3)	1.618(5)	–0.004
V(2)–O(5)	1.728(3)	1.716(6)	–0.012
V(2)–O(7)	1.835(3)	1.838(7)	0.003
V(2)–O(7)	1.961(3)	1.954(6)	–0.007
V(2)–O(10)	1.970(3)	1.966(7)	–0.004
V(3)–O(8)	1.738(2)	1.750(6)	0.012
V(3)–O(9)	1.735(3)	1.746(6)	0.011
V(3)–O(10)	1.732(3)	1.695(7)	–0.037
V(3)–O(11)	1.640(3)	1.649(6)	0.009

are 0.02 Å longer, the b axes 0.03 Å longer, and the c axes 0.1 Å shorter.

The average M(3)–O bond length of 2.048 Å for the distorted M(3)O₅ bipyramids in FeMg₂V₃O₁₁ is slightly shorter than the 2.057 Å for the ZnO₅ bipyramids in FeZn₂V₃O₁₁ (Table 4) but longer than the 1.943 Å for the FeO₅ bipyramids in FeVO₄. This agrees with the sizes and charges of the ions involved ($r(\text{Zn}^{2+}) > r(\text{Mg}^{2+}) > r(\text{Fe}^{3+})$) [22]. ZnO₅ trigonal bipyramidal coordination is rare but it has been observed in α -Zn₂V₂O₇ [28] and Ln₂BaZnO₅ [29]. The average V–O bond length of the V(2)O₅ bipyramids is 1.823 Å in FeMg₂V₃O₁₁ and 1.818 Å in FeZn₂V₃O₁₁. These values are close to the corresponding values of 1.813 Å in GaZn₂V₃O₁₁ and 1.819 Å in GaMg_{1.68}Zn_{0.32}V₃O₁₁. The bond angles for M(3)O₅ and V(2)O₅ bipyramids are given in Table 5. It can be seen that the largest bond angles, O(4)–M(3)–O(5) and O(7b)–V(2)–O(10), deviate from 180°, indicating that the cation is shifted from the center of the coordination environment.

Cation distribution is an important issue in the study of mixed metal oxides, particularly the study of multicomponent vanadate/molybdate catalysts. The specific disorder of the title compounds is not statistical and can be compared to several others in the literature. From the above discussions we know that Fe³⁺ and Mg²⁺ ions

Table 5
Selected bond angles(°) for $\text{FeMg}_2\text{V}_3\text{O}_{11}$ (M=Mg, Zn)

Bond angles	M=Mg	M=Zn	$\delta(\text{Zn-Mg})$
O(1)–M3–O(3)	116.2(1)	114.2(3)	–2.0
O(1)–M3–O(4)	93.0(1)	94.6(2)	1.6
O(1)–M3–O(5)	96.1(1)	98.5(2)	2.4
O(1)–M3–O(6)	131.9(1)	132.9(3)	1.0
O(3)–M3–O(4)	88.5(1)	85.9(2)	–2.6
O(3)–M3–O(5)	90.0(1)	88.1(2)	–1.9
O(3)–M3–O(6)	111.8(1)	112.9(3)	1.1
O(4)–M3–O(5)	170.6(1)	166.9(2)	–3.7
O(4)–M3–O(6)	91.3(1)	90.5(2)	–0.8
O(5)–M3–O(6)	80.7(1)	81.1(2)	0.4
O(4)–V(2)–O(5)	109.7(1)	108.9(3)	–0.8
O(4)–V(2)–O(7a)	116.6(1)	117.7(3)	1.1
O(4)–V(2)–O(7b)	102.0(1)	102.7(3)	0.7
O(4)–V(2)–O(10)	97.6(1)	96.4(3)	–1.2
O(5)–V(2)–O(7a)	133.3(1)	132.9(3)	–0.4
O(5)–V(2)–O(7b)	99.5(1)	99.7(3)	0.2
O(5)–V(2)–O(10)	94.4(1)	92.9(3)	–1.5
O(7a)–V(2)–O(7b)	77.2(1)	76.7(3)	–0.5
O(7a)–V(2)–O(10)	74.3(1)	76.6(3)	2.3
O(7b)–V(2)–O(10)	150.5(1)	152.2(3)	1.7

disorder on both the octahedral and bipyramidal sites of $\text{FeMg}_2\text{V}_3\text{O}_{11}$. A similar arrangement is found in W-type hexagonal ferrite $\text{BaMg}_2\text{Fe}_{16}\text{O}_{27}$ [30]. However, the bipyramidal M(3) site in $\text{FeMg}_2\text{V}_3\text{O}_{11}$ ($0.1\text{Fe}^{3+} + 0.9\text{Mg}^{2+}$) contains significantly more Mg^{2+} than the bipyramidal site in $\text{BaMg}_2\text{Fe}_{16}\text{O}_{27}$ ($0.92\text{Fe}^{3+} + 0.08\text{Mg}^{2+}$). This is surprising because trigonal bipyramidal coordination for Mg is uncommon, and yet the Mg^{2+} cations predominantly occupy this site in $\text{FeMg}_2\text{V}_3\text{O}_{11}$. Disorder between Fe^{3+} and Zn^{2+} is quite common and has been observed in both $\text{Sr}_2\text{Zn}_2\text{Fe}_{28}\text{O}_{46}$ (non-statistical) [31] and ZnFeBO_4 (statistical) [32].

The IR spectra for $\text{FeMg}_2\text{V}_3\text{O}_{11}$ and $\text{FeZn}_2\text{V}_3\text{O}_{11}$ are similar, and the absorptions are compared in Table 6. The absorptions below 700 cm^{-1} are equal within experimental error, but absorptions for the zinc analogue above 700 cm^{-1} are about $20\text{--}40\text{ cm}^{-1}$ lower in energy. This shift could not readily be explained by the differences of V–O bond lengths (see Table 4) but is consistent with the substantial difference in the melting points.

Plots of the reciprocal molar susceptibility ($1/\chi$) versus temperature (T) in the range of $50\text{--}300\text{ K}$ for both

Table 6
IR absorptions (cm^{-1}) for $\text{FeMg}_2\text{V}_3\text{O}_{11}$ and $\text{FeZn}_2\text{V}_3\text{O}_{11}$ ^a

$\text{FeMg}_2\text{V}_3\text{O}_{11}$	$\text{FeZn}_2\text{V}_3\text{O}_{11}$
1016 m	976 m
976 s	945 s
957 m sh	931 w sh
823 w sh	778 m sh
758 s br	726 s br
648 s	645 s
581 w sh	582 w sh
473 w br	475 w

^a s=strong, m=moderate, w=weak; br=broad, sh=shoulder.

$\text{FeMg}_2\text{V}_3\text{O}_{11}$ and $\text{FeZn}_2\text{V}_3\text{O}_{11}$ show Curie–Weiss behavior. The observed $\mu_{\text{eff}}=5.96\mu_{\text{B}}$ (spin-only calculated $\mu_{\text{eff}}=5.92\mu_{\text{B}}$) for both compounds reveals that the iron is exclusively high-spin d^5 . The negative Weiss constants ($\theta=-46.7\text{ K}$ for $\text{FeMg}_2\text{V}_3\text{O}_{11}$ and $\theta=-55.1\text{ K}$ for $\text{FeZn}_2\text{V}_3\text{O}_{11}$) indicate antiferromagnetic interactions between the Fe^{3+} ions as expected.

4. Conclusions

X-ray diffraction study of single crystal $\text{FeZn}_2\text{V}_3\text{O}_{11}$ and $\text{FeMg}_2\text{V}_3\text{O}_{11}$ reveals that they are isostructural with $\text{GaMg}_x\text{Zn}_{2-x}\text{V}_3\text{O}_{11}$ ($x=0, 1.7$). The Fe^{3+} , Mg^{2+} , and Zn^{2+} ions are found to disorder in their corresponding structures, and distributions on the octahedral and the trigonal bipyramidal sites are non-statistical. Variations in unit cell parameters between the two title phases result primarily from the distortion of the zinc octahedra. Infrared data agrees with the melting points and magnetic measurements confirm that Fe^{3+} is the only spin-magnetic species in each compound.

Acknowledgements

The authors wish to thank Dr. Claude Mertzénich and Dr. Larry Cirjak, and acknowledge an Extramural Research Award (EMRA) from BP America, Inc. and the National Science Foundation, Solid State Chemistry (award No. DMR-9412971 and DMR-9727516) for funding. This project made use of central facilities supported by the MRSEC program of the National Science Foundation (grant DMR-9632472) at the Materials Science Center of Northwestern University. DAVG is supported by a NSF graduate fellowship.

References

- [1] V.G. Zubkov, I.A. Leonidov, K.R. Poeppelmeier, V.L. Kozhevnikov, *J. Solid State Chem.* 111 (1994) 197.
- [2] X. Wang, C.L. Stern, K.R. Poeppelmeier, *J. Alloys Comp.* 243 (1996) 51.
- [3] X. Wang, K.R. Heier, C.L. Stern, K.R. Poeppelmeier, *J. Alloys Comp.* 255 (1997) 190.
- [4] X. Wang, K.R. Heier, C.L. Stern, K.R. Poeppelmeier, *J. Alloys Comp.* 267 (1998) 79.
- [5] W.D. Harding, H.H. Kung, V.L. Kozhevnikov, K.R. Poeppelmeier, *J. Catal.* 144 (1993) 597.
- [6] J.A. Ibers, J.W. Smith, *Acta Crystallogr.* 17 (1964) 190.
- [7] L. Katz, A. Kasenally, L. Kihlberg, *Acta Crystallogr. B* 27 (1971) 2071.
- [8] H. Szillat, H. Müller-Buschbaum, *Z. Naturforsch. B* 50 (1995) 247.
- [9] J.M. Hughes, S.J. Starkey, M.L. Malinconico, L.L. Malinconico, *Am. Mineral.* 72 (1987) 1000.
- [10] M.A. Lafontaine, J.M. Grenéche, Y. Lalignat, G. Férey, *J. Solid State Chem.* 108 (1994) 1.

- [11] X. Wang, D.A. Vander Griend, K.R. Poeppelmeier, *Inorg. Chem.* (1999) accepted.
- [12] L.N. Mulay, in: *Magnetic Susceptibility*, John Wiley and Sons, New York, 1963, p. 1782.
- [13] J. de Meulenaer, H. Tompa, *Acta Crystallogr.* 19 (1965) 1014.
- [14] G.M. Sheldrick, SHELXS86, in: G.M. Sheldrick, C. Krüger, R. Goddard (Eds.), *Crystallographic Computing 3*, Oxford University Press, 1985, p. 175.
- [15] P.T. Beurskens, G. Admiraal, G. Beurskens, W.P. Bosman, R. de Gelder, R. Israel et al., in: *The DIRDIF-94 Program System*, Technical Report of the Crystallography Laboratory, University of Nijmegen, The Netherlands, 1994.
- [16] TEXSAN: Crystal Structure Analysis Package, Molecular Structure Corporation, 1992.
- [17] C. Müller, H. Müller-Buschbaum, *J. Alloys Comp.* 191 (1993) 251.
- [18] C. Müller, H. Müller-Buschbaum, *J. Alloys Comp.* 185 (1992) 163.
- [19] M.M. Borel, A. Leclaire, J. Chardon, C. Michel, J. Provost, B. Raveau, *J. Solid State Chem.* 135 (1998) 302.
- [20] J. Darriet, J. Galy, *Cryst. Struct. Commun.* 2 (1973) 237.
- [21] B. Robertson, E. Kostiner, *J. Solid State Chem.* 4 (1972) 29.
- [22] R.D. Shannon, *Acta Crystallogr. A* 32 (1976) 751.
- [23] S. Busche, K. Bluhm, *Z. Naturforsch. B51* (1996) 671.
- [24] S. Boudin, A. Grandin, A. Leclaire, M.M. Borel, B. Raveau, *J. Solid State Chem.* 115 (1995) 140.
- [25] N.L. Ross, K. Leinenweber, *Z. Kristallogr.* 191 (1990) 93.
- [26] D.J. Lloyd, J. Galy, *Cryst. Struct. Commun.* 2 (1973) 209.
- [27] C. Gicquel-Mayer, M. Mayer, G. Perez, *Acta Crystallogr. B37* (1981) 1035.
- [28] R. Gopal, C. Calvo, *Can. J. Chem.* 51 (1973) 1004.
- [29] C. Michel, B. Raveau, *J. Solid State Chem.* 49 (1983) 150.
- [30] A. Collomb, O. Abdelkader, P. Wolfers, J.C. Guitel, *J. Magn. Magn. Mat.* 58 (1986) 247.
- [31] F. Leccabue, R. Panizzieri, G. Bocelli, G. Calestani, C. Rizzoli, N.S. Almodovar et al., *Magn. Mat.* 68 (1987) 365.
- [32] S. Busche, K. Bluhm, *Z. Naturforsch. B* 50 (1995) 1450.